Available online at www.CivileJournal.org

Civil Engineering Journal

(E-ISSN: 2476-3055; ISSN: 2676-6957)

Vol. 11, No. 12, December, 2025

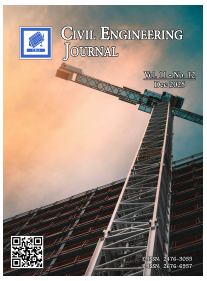

Probabilistic Reliability Framework for Nanomaterial-Stabilized Soft Clays: Model Calibration and Geometry Effects

Fawzi Kh. Khalaf [1, 2], Nur Irfah Mohd Pauzi [1], Mohammed Y. Fattah [3*], Karim Sherif Mostafa [4], Norbaya Sidek [5], Mohamed A. Hafez [6]

[1] *Civil Engineering Department, College of Engineering, Universiti Tenaga Nasional, 43000 Selangor, Malaysia.*

[2] *Department of Building and Construction Techniques Engineering, Madenat Alelem University College, 10006, Baghdad, Iraq.*

[3] *Faculty of Civil Engineering, University of Technology - Iraq, Al-Sina'a Street, Baghdad 10066, Iraq.*

[4] *Civil Engineering Discipline, School of Engineering, Monash University, Subang Jaya, Malaysia.*

[5] *School of Civil Engineering, College of Engineering, Universiti Teknologi MARA, Shah Alam 40450, Selangor, Malaysia.*

[6] *Department of Civil Engineering, Faculty of Engineering, FEQS INTI-IU, University, Nilai 71800, Malaysia.*

Received 23 July 2025; Revised 05 November 2025; Accepted 11 November 2025; Published 01 December 2025

Abstract

The stabilization of soft clay soils using nanomaterials offers a promising alternative to conventional additives such as lime and cement, yet most studies remain deterministic, neglecting soil variability and treatment geometry. This study proposes an experimental–probabilistic framework combining triaxial shear and model footing tests with Monte Carlo simulations to evaluate nano-SiO_2, nano-MgO, and nano-clay. Dosages from 1% to 5% were examined, and 3% was selected as optimal based on strength improvement and economic feasibility. Classical bearing capacity models (Terzaghi, Meyerhof, Hansen) were applied and calibrated using regression factors, with input variability modeled under normal and lognormal distributions. Results indicate that nano-MgO achieved the lowest probability of failure ($Pf < 0.1$), nano-SiO_2 showed intermediate but geometry-sensitive performance, and nano-clay provided limited reliability. The calibrated Terzaghi model ($R^2 = 0.742$) yielded the most consistent predictions. Enlarged treatment zones improved stress redistribution and reduced failure risk. The study also identifies priorities for future work: durability under cyclic loading, hybrid nanomaterial blends (e.g., SiO_2 + MgO), and scalability for large infrastructure projects. Collectively, the findings establish a reliability-based framework that integrates probabilistic modeling, calibration, and material geometry optimization for resilient geotechnical design.

Keywords: Nanomaterials; Soft Clay; Reliability; Monte Carlo; Durability; Bearing Capacity.

1. Introduction

In geotechnical engineering, stabilizing soft clay soils remains a major challenge due to their high compressibility, low shear strength, and sensitivity to moisture and loading changes. These issues often lead to excessive settlement and bearing capacity failure in critical infrastructure such as highways, embankments, and port facilities. While conventional

* Corresponding author: 40011@uotechnology.edu.iq

http://dx.doi.org/10.28991/CEJ-2025-011-12-03

chemical stabilizers like lime and cement have been widely used, recent advances in nanotechnology offer new possibilities. Nanomaterials such as nano-silica (SiO_2), nano-magnesium oxide (MgO), and nano-clay have shown promise due to their high surface area, pozzolanic activity, and efficiency at low dosages. Several studies have demonstrated performance improvements using nanomaterials.

For example, Gu et al. [1] reported a ~70% increase in unconfined compressive strength (UCS) using 1.5% nano-SiO_2. Hu et al. [2] showed better freeze thaw durability and reduced swelling with nano-MgO. Arabani et al. [3] achieved a 30% increase in bearing capacity using a combination of nano-clay and rice husk fibers. Similarly, Cheraghalikhani et al. [4] observed over a 40% improvement in California Bearing Ratio (CBR) using micro- and nano-bentonite, while P. Dukuly et al. [5] found enhanced compaction behavior from nano-silica inclusion.

Despite these promising results, current research has several critical limitations:

- Lack of uncertainty quantification – Most studies rely on deterministic designs, overlooking variability in soil properties such as cohesion (c), internal friction angle (φ), and unit weight (γ), which can lead to unsafe under design or overly conservative overdesign.
- No calibration of theoretical models with experimental data There is often a disconnect between laboratory results and theoretical design models.
- Limited focus on improvement zone geometry the width and depth of stabilized zones are typically held constant, even though geometry affects stress distribution and performance.

Some researchers have begun to explore probabilistic methods. Hassan Al-Riahi et al. [6], Pauzi et al. [7] applied Monte Carlo simulations to gypseous soils but did not integrate lab-based calibration. Sharmile et al. [8] reviewed nano-enhanced soils conceptually but without quantitative reliability modeling. Zhou et al. [9] focused on ductility gains in loess soils but ignored geometric variability and distribution assumptions. Furthermore, Lei et al. [10] studied nano-SiO_2-stabilized soils with fixed geometry, missing interactions between geometry and performance variability.

This study addresses these gaps through a combined experimental–probabilistic framework. Nano-treated soft clay soils using SiO_2, MgO, and clay are tested in the laboratory under varying treatment geometries. Strength parameters are evaluated through unconsolidated undrained triaxial tests, and ultimate bearing capacity is measured using model-scale footing tests. Classical bearing capacity models (Terzaghi, Meyerhof, Hansen) are calibrated using regression analysis, and variability is incorporated using Monte Carlo simulations to assess reliability metrics such as probability of failure (Pf) and reliability index (β).

The primary aim of this study is to establish a reliability-centered approach for the design of nano-stabilized foundations by integrating material science innovations with geotechnical risk analysis. A schematic overview of the adopted research methodology is provided in Figure 1, which illustrates the sequential stages of experimental investigation, theoretical modeling, statistical calibration, and probabilistic assessment.

2. Soil Sampling and Material Preparation

Undisturbed clay samples were collected from depths of 0.5 to 1.5 meters at the Grand Al-Fao Port site in Basra, Iraq, using auger drilling to maintain the natural structure and in-situ properties of the soil. The collected samples were initially in a plastic state and were air-dried at room temperature for 24 hours, followed by oven-drying at 105 °C until a constant mass was reached. The dried material was then crushed and pulverized to achieve a uniform fine powder. This was followed by blending with nano-silica (SiO_2), nano-magnesium oxide (MgO), and nano-clay at varying dosages between 1% and 5% by dry weight. Mechanical mixing was conducted for 10 minutes to ensure uniform dispersion of the nanomaterials and minimize agglomeration. The mixtures were then cured for 24 hours to allow for preliminary physicochemical interaction prior to testing. The sequential stages of this preparation process from raw clay to powdered, nano-treated material is illustrated in Figure 2.

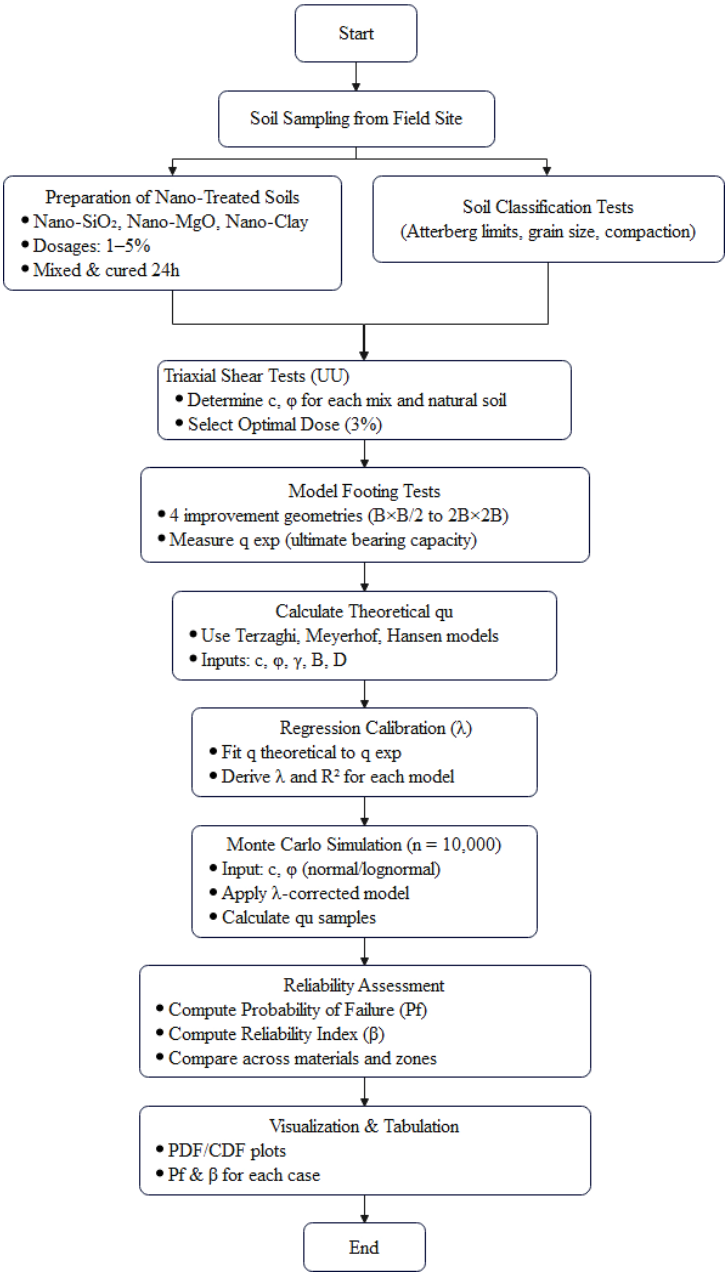

Figure 1. Flowchart of the Experimental and Probabilistic Framework for Nano-Stabilized Soft Clay Foundations

Figure 2. Sequential Stages of Soil Sample Preparation (A) Jaw crusher, (B) Raw clay, (C) Grinder and mixer, (D) Powdered soil

3. Overview of Experimental Design

To evaluate the Geomechanical behavior of nanomaterial-treated clay soils, the experimental program was conducted in three stages: classification tests, triaxial shear tests, and model footing tests. First, standard classification tests including Atterberg limits, compaction, specific gravity, and grain size analysis were performed to characterize the treated soils and establish a consistent baseline. Then, 45 consolidated drained triaxial tests were conducted to assess changes in cohesion (c) and internal friction angle (ϕ) at nanomaterial dosages ranging from 1% to 5% for Nano Clay, Nano MgO, and Nano SiO_2. Based on the results, 3% was selected as the optimal dosage due to its strength improvement and practical feasibility. Finally, 13 model footing tests were carried out to study the effects of nanomaterial type and treatment geometry on bearing capacity and load–settlement behavior under shallow foundations.

3.1. Triaxial Testing (UU Method)

To assess the short-term shear strength behavior of nano-treated clays under undrained conditions, Unconsolidated Undrained (UU) triaxial compression tests were performed in accordance with ASTM D2850-07. Specimens prepared at optimum moisture content and maximum dry density were subjected to confining pressures of 200, 300, and 400 kPa, followed by axial loading at a constant strain rate until failure. The resulting data enabled the determination of cohesion (c) and internal friction angle (f). Nanomaterials (Nano Clay, Nano MgO, and Nano SiO_2) were introduced to improve interparticle bonding and structural integrity. The testing simulated rapid loading scenarios, where no drainage occurs, reflecting conditions typical of sudden load applications in the field. Uniform sample preparation was ensured via controlled tamping, dimensional checks, and membrane sealing. The findings provide critical insight into the undrained shear strength enhancement achieved through nanomodification, offering guidance for improving the immediate load-bearing performance of soft clay soils.

3.2. Foundation Model for Nano-Improved Soils

Undisturbed clay samples were extracted from boreholes at the Grand Al-Faw Port site (Basra, Iraq) at depths of 0.5–1.5 m to capture key geotechnical layers. Auger drilling was employed to minimize disturbance and preserve the natural structure. The soil was oven-dried at 110 ± 5 °C, pulverized, and characterized in accordance with ASTM standards.

- Three Nanomaterials were used as Stabilizers:
  - Montmorillonite-based Nano Clay
  - Nano Magnesium Oxide (Nano-MgO)
  - Nano Silicon Dioxide (Nano-SiO_2)

A fixed dosage of 3% by dry weight selected based on triaxial test performance and economic viability—was thoroughly blended with designated soil portions using a mechanical mixer for 10 minutes, followed by a 24-hour equilibration period at ambient conditions.

- Physical Model Configuration

A rigid steel test box (90 × 45 × 30 cm) was used to simulate shallow foundation behavior under controlled conditions. A 4 × 4 cm square footing was centrally placed at the soil surface as shown in Figure 3. Four improvement geometries were tested (Table 1), each representing varying reinforcement zones beneath the footing.

(a) (b)

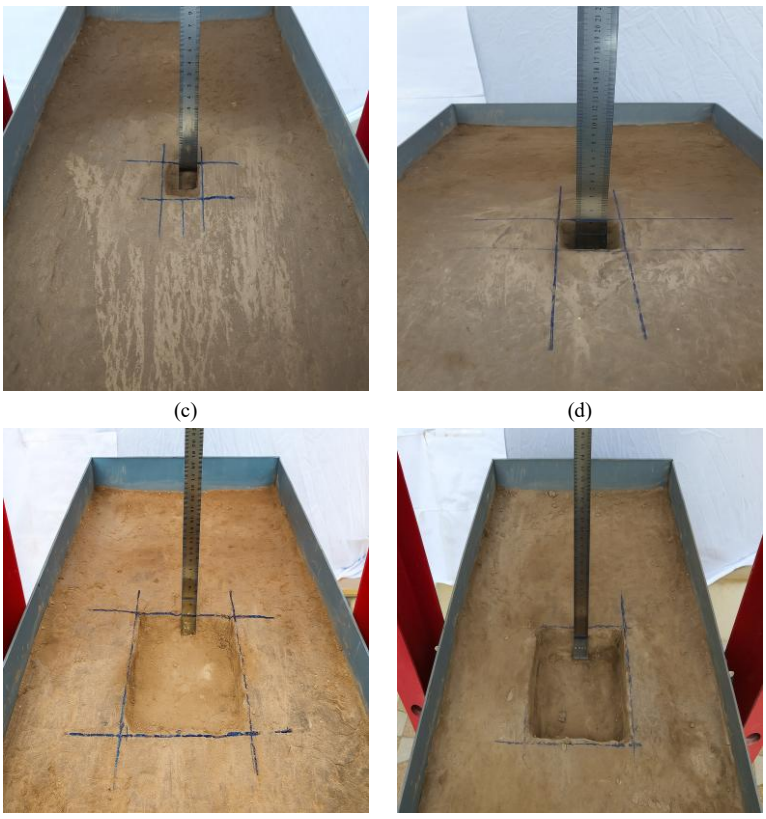

(c) (d)

(e) (f)

Figure 3. a) Placing the initial soil layer and marking compaction levels. b) Leveling the compacted soil surface, c) Marking the improved zone boundaries for Case 1, d) Marking the improved zone boundaries for Case 2, e) Marking the improved zone boundaries for Case 3, f) Marking the improved zone boundaries for Case 4.

Table 1. Geometric Configurations of Improved Soil Zones Beneath the Footing

Case	Improved Zone Width (cm)	Improved Zone Depth (cm)	Geometric Representation (relative to B)
1	4	2	B × B/2
2	4	4	B × B
3	8	2	2B × B/2
4	8	4	2B × B

Note: B = 4 cm (footing width). Each scenario was tested for all three nanomaterials and compared with untreated natural soil.

- Compaction and Layering

Each test box was filled in five 5-cm layers, compacted to reach the optimum dry density (ODD) and optimum moisture content (OMC) determined from Proctor tests. Dry mass was calculated volumetrically, and moisture content was adjusted accordingly. Each layer was compacted and leveled before the next was placed, with random density verification samples taken to ensure uniformity.

- Footing Installation and Instrumentation

The model footing was placed centrally on the prepared soil surface. Dial gauges were mounted on both sides to measure settlements, with a seating load of 5 kN/m² applied for 24 hours to stabilize the setup before testing as shown in Figure 4.

- Loading Procedure
  - Vertical loads were applied incrementally using a calibrated hydraulic system:
  - Initial Stage: 10% of estimated ultimate capacity
  - Intermediate Stage: Increased to 20% if response was linear
  - Final Stage: Reverted to 10% if nonlinear behavior was observed
  - Each load increment was maintained for 18 minutes, and settlement readings were recorded at each stage in compliance with ASTM D1194-94.

- Failure and Data Interpretation

Failure was defined as settlement equal to 10% of footing width (4 mm). Load corresponding to this settlement was recorded as the ultimate bearing capacity. Load–settlement curves were plotted for all test cases to assess the impact of nanomaterials on both capacity and stiffness.

- Quality Assurance

All procedures adhered to ASTM standards and Alshami et al. [11]. Equipment was calibrated before use, and all experiments were documented through photographs and digital logs. Select tests were repeated to ensure reproducibility and data integrity.

Figure 4. Model Footing Test Apparatus with Labeled Components (1- Hydraulic Press, 2- Dial Gauge, 3- Loading Plate Connection, 4- Load Cell, 5- Model Footing, 6- Manual Jack Handle, 7- Uninterruptible Power Supply, 8- Load indicator)

4. Reliability Analysis of Bearing Capacity for Nano-Treated Soils

To evaluate the structural reliability of foundations over nano-treated clay soils, a probabilistic framework was developed that integrates experimental data with classical theoretical models, statistical calibration, and Monte Carlo simulations. By Phoon & Tang [12], and later by Baecher [13]. This section outlines the methodology used to compute the Probability of Failure (Pf) and Reliability Index (β) under varying soil improvements and design conditions.

- Statistical Modeling of Shear Strength Parameters

The two primary input variables Cohesion (c) and Internal Friction Angle (ϕ) were derived from unconsolidated undrained (UU) triaxial test results. To incorporate inherent material variability, each parameter was modeled as a random variable. Two probabilistic scenarios were considered:

○ *Normal Distribution:*

$$c \sim N(\mu_c, \sigma_c^2), \phi \sim N(\mu_\phi, \sigma_\phi^2),\ c \sim \phi \quad (1)$$

○ *Lognormal Distribution for Cohesion:*

$$N(\mu_c, \sigma_c^2) \sim Lognormal(\mu_{lnc}, \sigma_{lnc}),\ c \sim \phi \quad (2)$$

A coefficient of variation (COV) of 10% was assumed for both parameters to reflect moderate experimental uncertainty.

- Theoretical Bearing Capacity Calculation

For each simulation (n = 10,000 samples), random values of C_i and ϕi were generated and applied to compute the ultimate bearing capacity using the Terzaghi, Meyerhof, or Hansen models:

$$qu_i = c_i N_c + \gamma_d N_q + 0.5\gamma B N_\gamma \quad (3)$$

where the bearing capacity factors $Nq, Nc, N\gamma$ are functions of ϕ, defined as:

$$Nq = exp(\pi tan\phi_i)[tan(4\pi + 2\phi_i)]^2, Nc = tan\phi_i N_q - 1, N_\gamma = 2(Nq + 1)tan\phi_i \quad (4)$$

These calculations were repeated for each of the 13 experimental cases across different nanomaterials and geometric configurations.

- Regression Calibration and Limit State Function

To reconcile theoretical predictions with experimental results, a regression-based correction factor (λ) was applied:

$$qu_{\text{corr}} = \lambda \cdot qu_{\text{Terzaghi}}$$

The optimal λ and coefficient of determination R^2 were determined for each model, with the highest R^2 model selected for reliability assessment.

A limit state function was defined as:

$$G_i = qu_{corr,i} - qu_{exp} \quad (5)$$

Failure occurs when $G_i < 0,\ i.e.\ qu_i < qu_{exp}$., i.e., when the predicted capacity is lower than the experimental demand.

- Reliability Metrics

Probability of Failure (Pf) was estimated as the fraction of simulations where $G_i < 0$:

$$Pf = \frac{(qu_i < qu_{exp})}{N_{sim}} \quad (6)$$

Reliability Index (β), a standard reliability metric, was computed as:

$$\beta = -\Phi^{-1}(Pf) \quad (7)$$

where Φ^{-1} is the inverse cumulative distribution function (CDF) of the standard normal distribution.

- Model Selection and Sensitivity

Among the models evaluated (Terzaghi, Meyerhof, Hansen), the one yielding the highest R^2 after calibration was selected as the reliability basis. Sensitivity to parameter distribution was assessed by comparing Normal and Lognormal assumptions.

5. Results and Discussion

5.1. Baseline Properties of Untreated Clayey Soil

The clay soil sample underwent comprehensive physical and chemical testing to evaluate its properties for potential stabilization applications. The grain size distribution, illustrated in Figure 5 and summarized in Table 2, indicates a composition of 60% silt and 40% clay. This composition is associated with the soil's high plasticity and expansive behavior. Based on Atterberg limits liquid limit (47%), plastic limit (20.5%), and plasticity index (26.5%), the soil is classified as high-plasticity clay (CH) according to the Unified Soil Classification System (USCS) in compliance with ASTM D2487. Additionally, a shrinkage limit of 10.8% indicates moderate dimensional stability during drying.

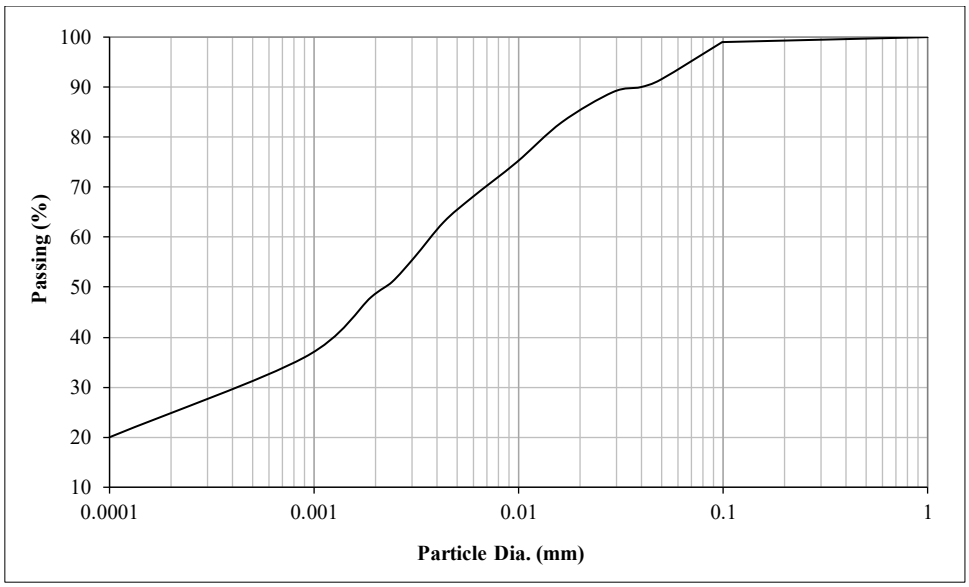

Figure 5. Grain size distribution for clay soil sample

Table 2. Index Properties and Classification of Clay Soil Sample

Index Property	Index Value	Standard Specification
Specific gravity (Gs)	2.661	ASTM D854-14 [14]
Silt (0.005 to 0.075 mm) (M) %	60	ASTM D422-63(2007) [15]
Clay (less than 0.005mm) (C) %	40	ASTM D422-63(2007) [15]
Liquid limit (%)	47	ASTM D4943-08 [16]
Plastic limit (%)	20.5	ASTM D4943-08 [16]
Plasticity index (%)	26.5	-
shrinkage limit ($L.Sh.$) %	10.8	ASTM D4318-00 [17]
Optimum Moisture Content (O.M.C) (%)	20.2	ASTM D698-12(2021) [18]
Maximum Dry Density (MDD) kN/m^3	15.6	ASTM D698-12(2021) [18]
Classification according to the (USCS)	CH	ASTM D2487-17e1 [19]

Compaction characteristics, derived from the compaction curve in Figure 6, reveal an optimum moisture content (OMC) of 20.2% and a maximum dry density (MDD) of 15.6 kN/m³, determined according to ASTM D698. These values represent the moisture content at which the soil achieves its highest compaction, a critical parameter for assessing its suitability for construction applications.

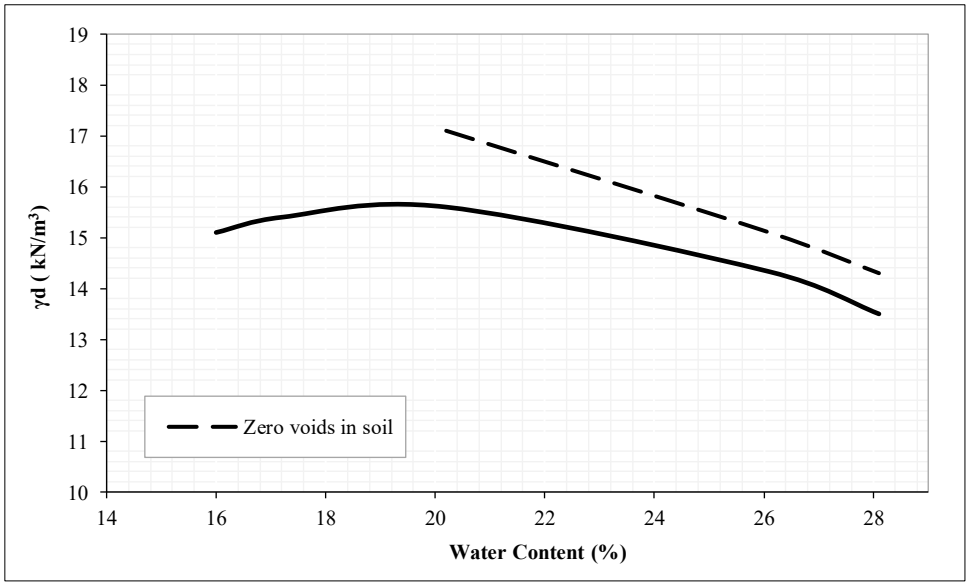

Figure 6. Compaction curve for clay soil sample

The chemical properties, summarized in Table 3, provide additional insights into the soil's behavior and potential challenges for structural applications. Key findings include a sulphate content of 0.94% (ASTM D516), gypsum content of 2.72% (BS 1377-1990), total suspended solids (TSS) of 7.62% (ASTM D1888), chloride content of 2.4% (ASTM D4327), and organic matter content of 3.9% (ASTM D2974). These values are significant for evaluating potential risks such as soil corrosion and compatibility with stabilization additives.

Table 3. Chemical Properties of Clay Soil Sample.

Chemical Properties	Test Results	Standard Specification
Sulphate Content (SO_4) %	0.94	BS 1377: 1990 [20]
Gypsum Content (Gyp) %	2.72	Head & Epps [21]
Total Suspended Solids (T.S.S.) %	7.62	ASTM D5907-18 [22]
Chloride Content (Cl) %	2.4	ASTM D512-23 [23]
Organic Matter (Org) %	3.9	ASTM D2974-14 [24]

5.2. Shear Strength Parameters of Nano-Modified Soils

Shear strength is a fundamental parameter governing the stability and load-bearing behavior of geotechnical systems. In this study, the Unconsolidated Undrained (UU) triaxial tests was used to evaluate the mechanical response of soft clay treated with nanomaterials: Nano-SiO_2, Nano-MgO, and Nano-clay. As shown in Table 4, all nanomaterials contributed to improvements in cohesion (c) and friction angle (φ), alongside noticeable changes in maximum dry density (γd_{ax}) and optimum moisture content (OMC). Among the three additives, nano-MgO yielded the highest cohesion values, reaching 220 kPa at 5% dosage, accompanied by moderate gains in φ. These enhancements are attributed to the formation of magnesium silicate hydrate (M–S–H) and brucite, which improved chemical bonding and microstructural densification. Similar findings were reported by Kalhor et al. [25], who observed improved freeze–thaw resistance and reduced swelling in MgO-treated clays.

Table 4. Influence of Nanomaterials on Shear Strength.

Material	Percentage (%)	γd_{Max} (kN/m^3)	OMC (%)	Coherence (kPa)	Friction Angle (φ°)
Soft Clay	*0*	*16.8*	*22.5*	*42*	*6.3*
Nano SiO_2	*1*	17.6	23.8	110	7.4
Nano SiO_2	*2*	18.2	24.5	125	8
Nano SiO_2	*3*	18.4	25	140	8.7
Nano SiO_2	*4*	18.5	25.5	170	9.5
Nano SiO_2	*5*	16.8	22.5	195	10.2
Nano MgO	*1*	17.2	23.3	125	7.2
Nano MgO	*2*	17.9	24.5	150	7.6
Nano MgO	*3*	18.5	25.1	180	7.9
Nano MgO	*4*	18.7	25.5	200	8.3
Nano MgO	*5*	18.8	26.4	220	8.5
Nano Clay	*1*	16.5	22.3	52	۶٫۵
Nano Clay	*2*	17.2	23.5	81	6.7
Nano Clay	*3*	17.9	25.1	105	7
Nano Clay	*4*	18.5	25.5	130	7.3
Nano Clay	*5*	18.1	26.2	150	7.5

Nano-SiO_2 also produced substantial gains, with cohesion increasing from 42 kPa (untreated) to 195 kPa (5%), and friction angle rising from 6.3° to 10.2°. These effects are primarily due to pozzolanic reactions and the formation of calcium silicate hydrate (C–S–H) gels, in addition to the high surface reactivity of SiO_2. This trend aligns with the results of Ibrahim et al. [26], who reported up to a 70% increase in UCS with 1.5% nano-SiO_2 addition. In comparison, nano-clay showed moderate improvements in strength parameters, reaching 150 kPa cohesion and 7.5° friction angle at 5%, mainly through physical intercalation and swelling behavior rather than chemical bonding. Abdulamer & Daham [27] similarly found modest strength gains using nano-clay combined with rice husk fibers. Overall, the results confirm a direct relationship between nanomaterial dosage and shear strength enhancement, particularly for pozzolanic-active additives (SiO_2 and MgO), which also led to increased dry densities and OMC values key indicators of better compaction and improved soil structure. These trends are detailed in Table 4.

5.3. Friction Angle Behavior (φ)

In addition to cohesion, the internal friction angle (φ) of the treated soft clay exhibited notable, though comparatively moderate, improvements across all nanomaterials. As illustrated in Figure 7, the upward shift in the Mohr–Coulomb failure envelopes confirms the enhanced shear resistance resulting from nanomaterial inclusion.

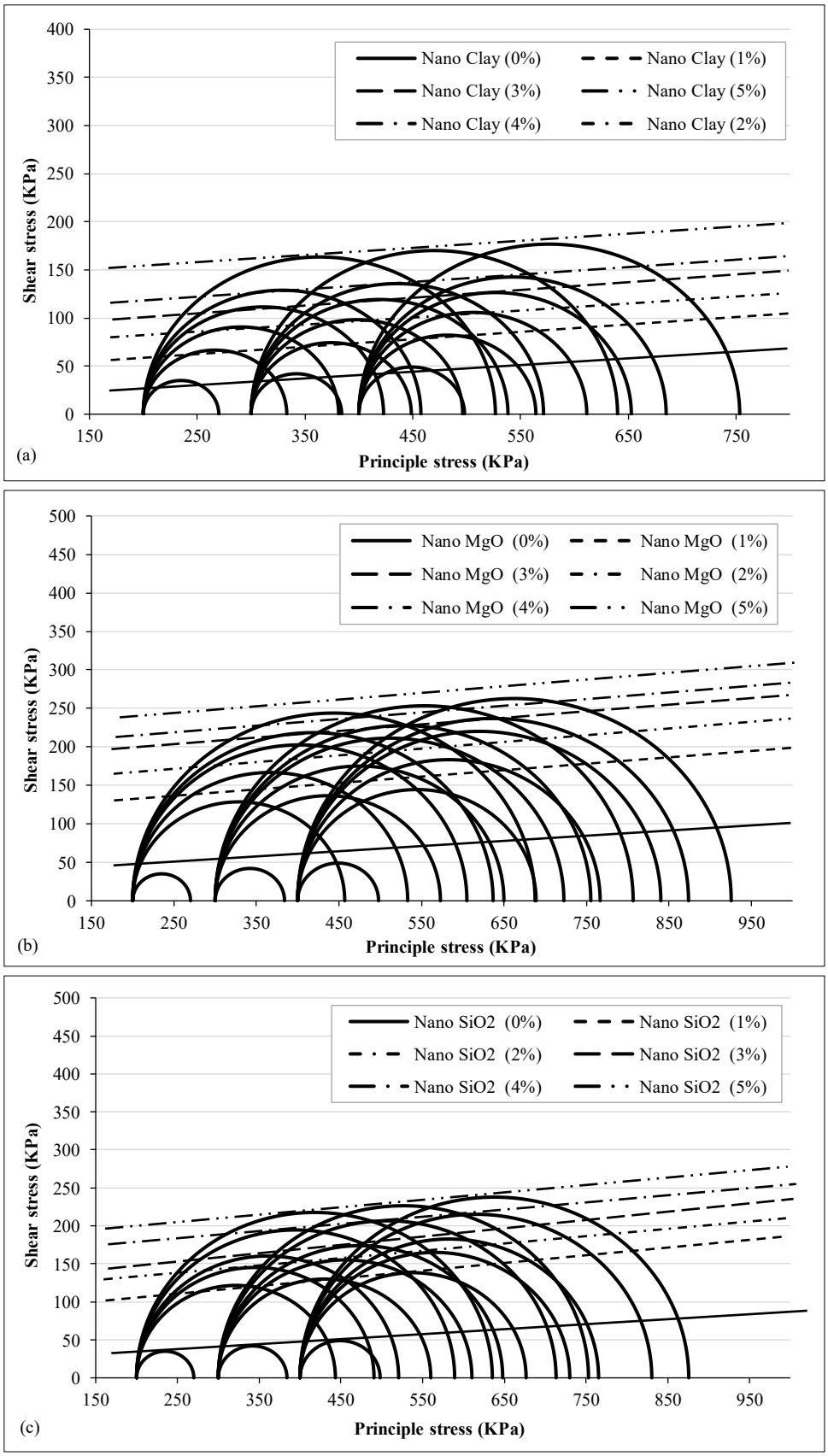

Figure 7. Mohr–Coulomb Failure Envelopes for Soft Clay Treated with Varying Percentages of (A) Nano Clay, (B) Nano MgO, (C) Nano SiO_2

Nano-SiO_2 showed the most significant increase in φ, from 7.4° to 10.2°, representing an approximate 38% enhancement (Figure 7-C). This improvement is attributed to microstructural densification, stronger particle interlocking, and increased surface roughness due to siloxane bonding and the formation of cementitious gels that reduce slippage within the soil matrix.

Nano-MgO demonstrated a consistent increase in φ, ranging from 7.2° to 8.5° (Figure 7-B), owing to the formation of magnesium silicate hydrate (M–S–H) phases. These contribute to greater angularity and contact between soil particles, leading to higher resistance to shear deformation.

Nano-Clay showed a modest increase in φ, from 6.5° to 7.5° (Figure 7-A). The limited enhancement is likely due to the plate and laminar structure of clay minerals, which promotes sliding and restricts the development of strong interparticle friction or binding gels, even after treatment.

These results affirm that while all nanomaterials improve friction angle to some degree, pozzolanic-reactive materials such as Nano-SiO_2 and Nano-MgO are more effective in enhancing interparticle friction through chemical bonding and matrix densification.

5.4. Selection of 3% as the Optimal Nanomaterial Dosage

The selection of the 3% nanomaterial dosage was significantly influenced by economic considerations. Given that the local market cost of nanomaterials in Iraq exceeds $1,000 per kilogram, careful economic evaluation is critical. Experimental results revealed that increasing the nanomaterial dosage from 3% to 5% resulted in only minor incremental improvements for instance, cohesion increased by approximately 8–15% (from 180 kPa at 3% to 195–220 kPa at 5%), and the maximum dry density improved by just 1–2% (from 18.5 kN/m³ at 3% to 18.8 kN/m³ at 5%). In contrast, the associated material costs rose disproportionately (approximately 66% higher), making such marginal enhancements economically unjustifiable.

Conversely, dosages below 3% (such as 1% or 2%) yielded substantially reduced geotechnical benefits, potentially leading to inadequate soil stabilization and higher long-term maintenance costs. For example, at 1–2% dosage, cohesion values ranged from only 81 to 150 kPa, representing a significant reduction in stabilization effectiveness compared to the optimal 3% dosage (140–180 kPa). Consequently, adopting a 3% dosage was determined to offer the optimal balance, ensuring significant improvements in soil properties at a justifiable economic investment, thus achieving maximum cost-efficiency and structural reliability.

5.5. Performance Evaluation of Nano-Treated Soils

The experimental results clearly demonstrate the positive impact of nanomaterial incorporation on the mechanical behavior of soft clay soils under shallow foundations. As illustrated in Figure 8 and detailed in Table 5, all nanomaterial types Nano SiO_2, Nano MgO, and Nano Clay led to substantial improvements in ultimate bearing capacity ($qu_{(max)}$) across all treatment cases (Cases 1–4), compared to untreated natural soil.

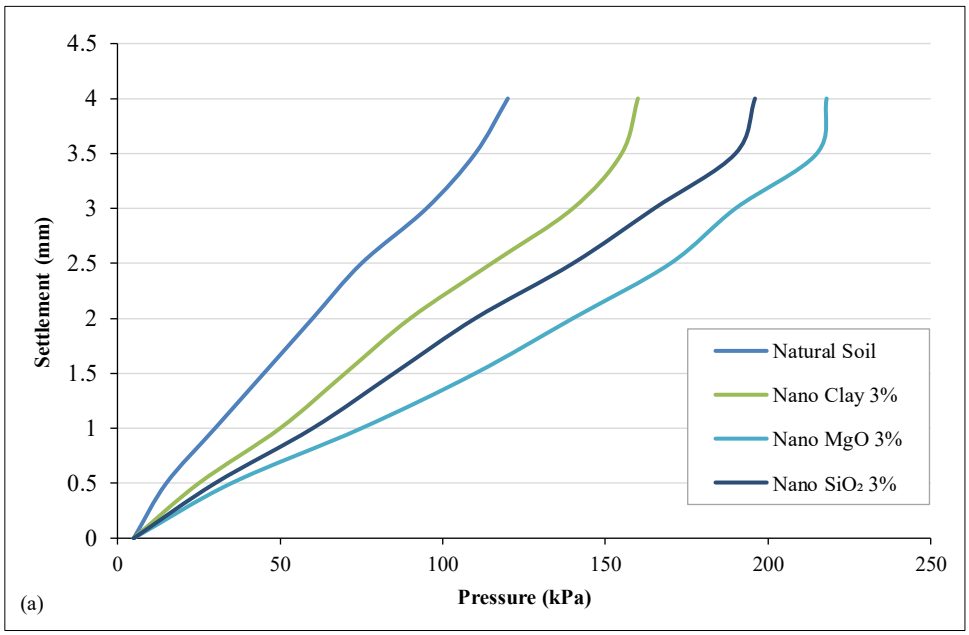

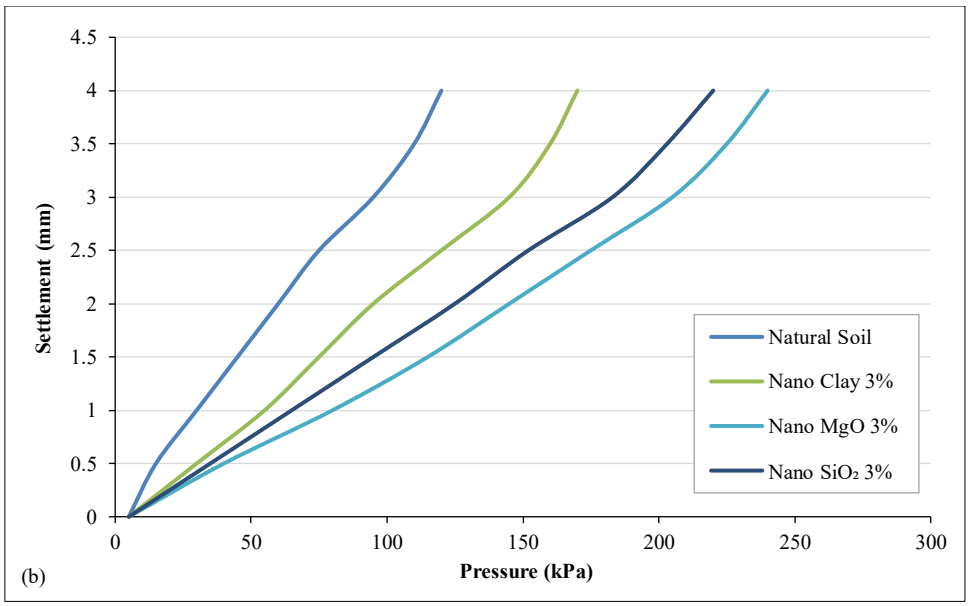

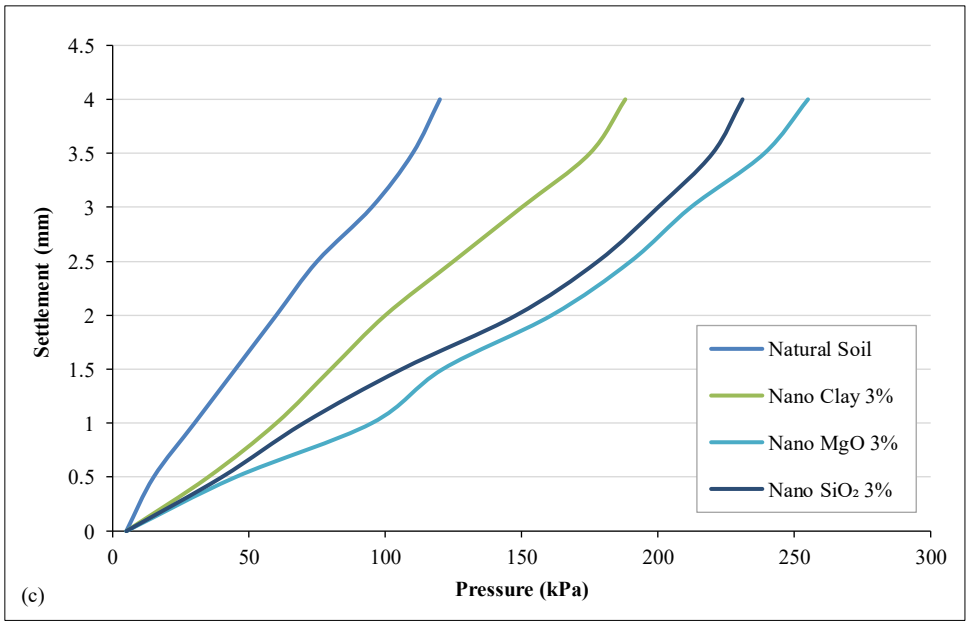

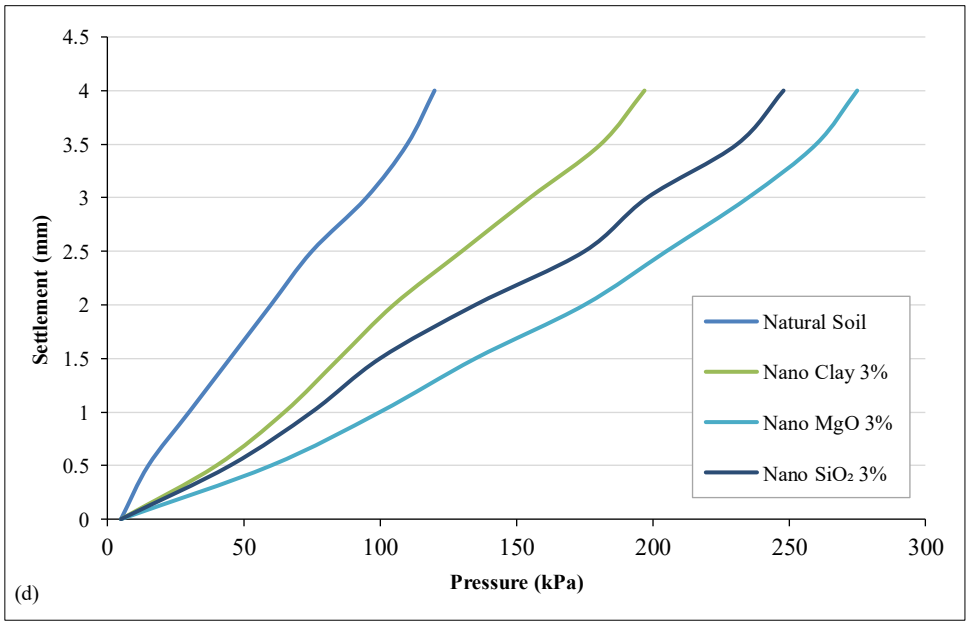

Figure 8. Load–settlement behavior for natural and nano-treated soils with 3% nanomaterials under different treatment geometries: (a) Case 1, (b) Case 2, (c) Case 3, (d) Case 4

Table 5. Mechanical Performance of Nano-Treated Soils under Various Foundation Cases

Nanomaterial	Case	qu_{ult} Kpa	Δqu_{ult} (%)	I_T	$K_s(kPa/mm)$	K_{rel}
Natural Soil	All	120	—	1.00	30	1.00
Nano Clay 3%	Case 1	160	33.3%	1.33	45	1.50
	Case 2	170	41.7%	1.42	47.5	1.58
	Case 3	188	56.7%	1.57	50	1.67
	Case 4	197	64.2%	1.64	51.5	1.72
Nano MgO 3%	Case 1	218	81.7%	1.82	55	1.83
	Case 2	240	100.0%	2.00	57.5	1.92
	Case 3	255	112.5%	2.13	64	2.13
	Case 4	275	129.2%	2.29	66	2.20
Nano SiO_2 3%	Case 1	196	63.3%	1.63	70	2.33
	Case 2	220	83.3%	1.83	72.5	2.42
	Case 3	231	92.5%	1.93	74	2.47
	Case 4	248	106.7%	2.07	75	2.50

NOT: ([Bearing Capacity – $qu_{ult} = I_T \times q_{nat}$], [Percentage Improvement(Δqu_{ult} %) = $\frac{qu_{nat(ult)-q}}{qu_{nat}} \times 100$], [Relative Bearing Index (I_T) = $\frac{qu_{ult}}{qu_{nat}}$], [Stiffness Modulus ($K_s$) = $\frac{\Delta q}{\Delta S}$], [Relative Stiffness Index (K_{rel}) = $\frac{K_s}{K_{s(natural)}}$]).

Among the treatments, Nano SiO_2 yielded the highest bearing capacity, reaching 248 kPa in Case 4, a 103.7% increase relative to the baseline (120 kPa). Nano MgO and Nano Clay followed with maximum improvements of 83.7% and 45.9%, respectively. These trends are clearly visualized in Figure 9, which highlights the comparative performance of the three nanomaterials across all improvement geometries. The figure shows a consistent and progressive increase in bearing capacity with both material reactivity and treatment geometry, confirming the effectiveness of Nano SiO_2 in particular. These gains are attributed to two synergistic mechanisms:

- ***Material Reactivity***: The high pozzolanic and micro-filling potential of Nano SiO_2 enhances interparticle bonding and densifies the soil matrix through the formation of C–S–H gels.
- ***Geometric Optimization***: Increasing the width and depth of the treated zone allows for better stress distribution and mobilization of improved soil volume, further delaying failure.

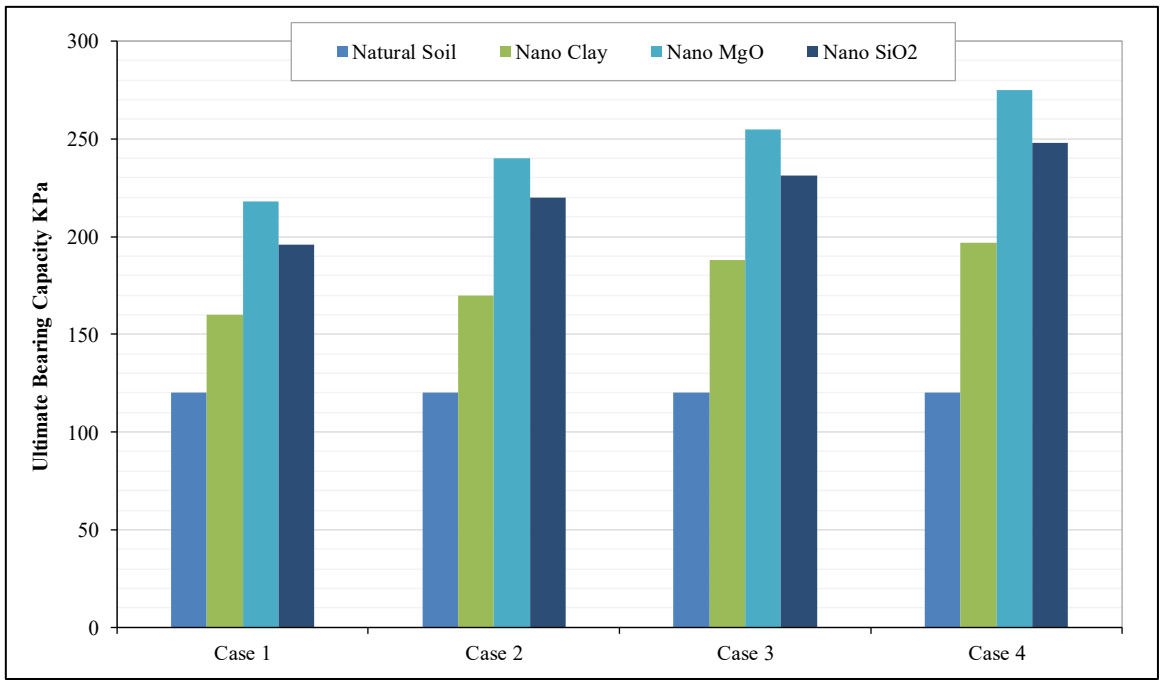

Figure 9. Variation of Ultimate Bearing Capacity with Nanomaterial Type and Improvement

In addition to strength gains, the Relative Stiffness Index (K_{rel}) also increased systematically with nanomaterial reactivity and treatment geometry. As seen in Table 5, Nano SiO_2 treatments reached a maximum (K_{rel}) = 2.50, compared to 2.20 for Nano MgO and 1.72 for Nano Clay. These enhancements are not solely due to increased strength but also reflect improved load–settlement behavior, particularly the steeper initial slopes observed in Figure 8 (A to D),

indicating higher resistance to early-stage deformation. This performance is a direct result of microstructural refinement including pore filling, particle interlocking, and the formation of cementitious bonds which is particularly pronounced with high-reactivity materials like Nano SiO_2. From an engineering standpoint, these improvements translate into:

- Reduced serviceability settlements under working loads,
- Enhanced reliability and safety of shallow foundations,
- And greater flexibility in designing infrastructure over soft clay deposits.

5.6. Comparative Performance and Mechanisms of Nanomaterials

The comparative analysis presented in Figure 10 (radar chart of relative stiffness index) and Figure 11 (bar chart of ultimate bearing capacity) highlights a consistent performance hierarchy among the tested nanomaterials:

- Nano-SiO_2 > Nano-MgO > Nano-Clay

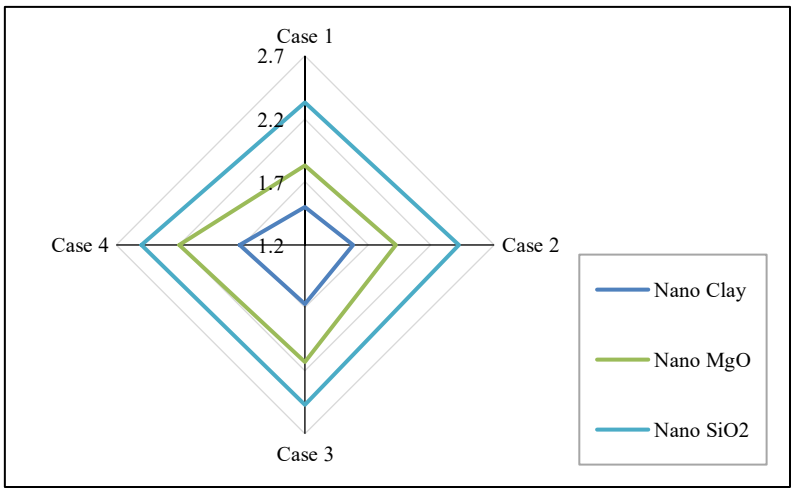

Figure 10. Effect of Nanomaterial Type on Relative Stiffness Index under Different Scenarios

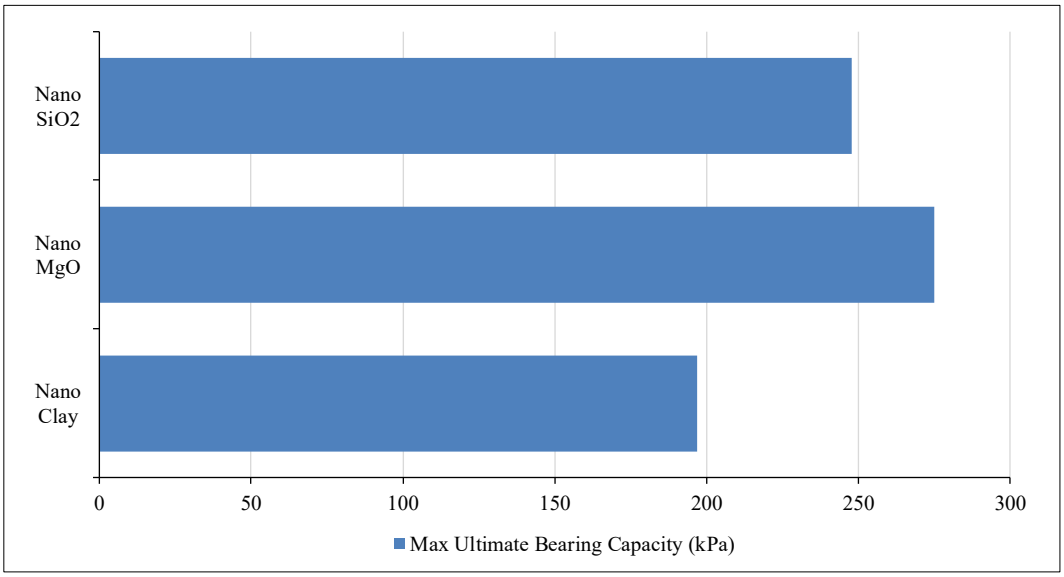

Figure 11. Max Ultimate Bearing Capacity with Different Nanomaterials

Nano-SiO_2 exhibited the highest improvement across all performance metrics, attributed to its ultra-fine particle size, high specific surface area, and strong pozzolanic reactivity, which together facilitate rapid formation of calcium silicate hydrate (C–S–H) gels. These gels enhance matrix density and interparticle bonding, resulting in superior mechanical behavior. Similar observations were reported by Regalla [28], who found significant increases in strength and stiffness in clayey soils treated with nano-silica. Cheraghalikhani et al. [4] also noted over 40% improvement in California Bearing Ratio (CBR) when using micro- and nano-bentonite, attributing gains to enhanced gel formation and reduced pore continuity.

Nano-MgO, though less reactive, still delivered substantial improvements due to its ability to form magnesium silicate hydrate (M–S–H) phases and refine soil microstructure. This aligns with findings by Yao et al. [29], who

demonstrated improved freeze–thaw durability and microstructural densification in MgO-treated soils. Nano-Clay, while the least reactive, provided measurable gains—particularly relevant in cost-sensitive applications or where material availability is limited. Khayat et al. [30] reported modest strength increases when combining nano-clay with rice husk fibers, especially in low-cost or resource-constrained settings. The improvements observed in both bearing capacity and stiffness are not purely numerical but stem from identifiable mechanistic transformations in the treated soils. Nanomaterial inclusion:

- Reduces pore size and continuity, limiting moisture migration and collapse potential.
- Strengthens interparticle contacts, enhancing both initial stiffness and ultimate load capacity.

Modifies failure behavior, shifting the response from ductile to semi-brittle, enabling higher design safety margins without compromising serviceability. These findings have clear practical implications. From a design perspective, they enable engineers to strategically select nanomaterials and tailor treatment geometries to balance performance objectives with cost and material constraints. While nano-SiO_2 offers the highest performance for critical infrastructure on soft clays (e.g., coastal foundations), nano-MgO and nano-clay remain viable alternatives for projects requiring moderate improvement at lower cost.

6. Reliability Analysis Results

6.1. Influence of Model Selection, Distribution Type, and Calibration on Bearing Capacity Predictions

The comparative analysis of classical bearing capacity formulations reveals that the accuracy and reliability of predicted ultimate capacity (qu) in nanomaterial-treated soils are strongly governed by three interdependent factors: model architecture, probabilistic representation of input variables, and statistical calibration. The choice of analytical model dictates the baseline conservatism of predictions. Terzaghi's formulation consistently produces the lowest mean capacities with the narrowest probability density functions (PDFs), reflecting its structural simplicity and omission of geometric and load-inclination factors. In contrast, Hansen's formulation yields the highest mean capacities and widest distributions, due to its comprehensive incorporation of shape, depth, and loading parameters. While this sophistication broadens predictive flexibility, it also amplifies sensitivity to uncertainties in cohesion (c) and internal friction angle (φ), as evidenced by the longer-tailed distributions (Figures 12 and 13). Meyerhof's formulation generally occupies an intermediate position but tends to converge toward Hansen under high cohesion values, illustrating its semi-empirical balance between robustness and responsiveness to parameter variability.

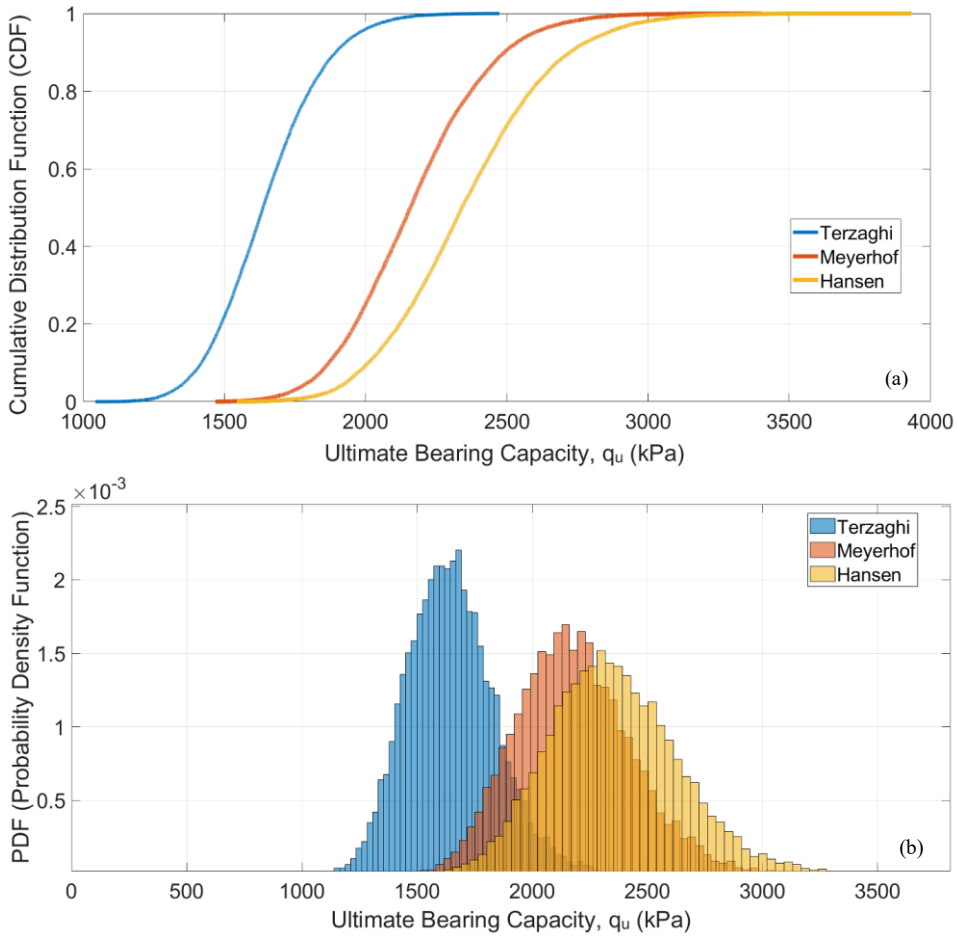

Figure 12. Lognormal distribution of cohesion (c): (a) uncorrected PDF curve, (b) uncorrected CDF curve

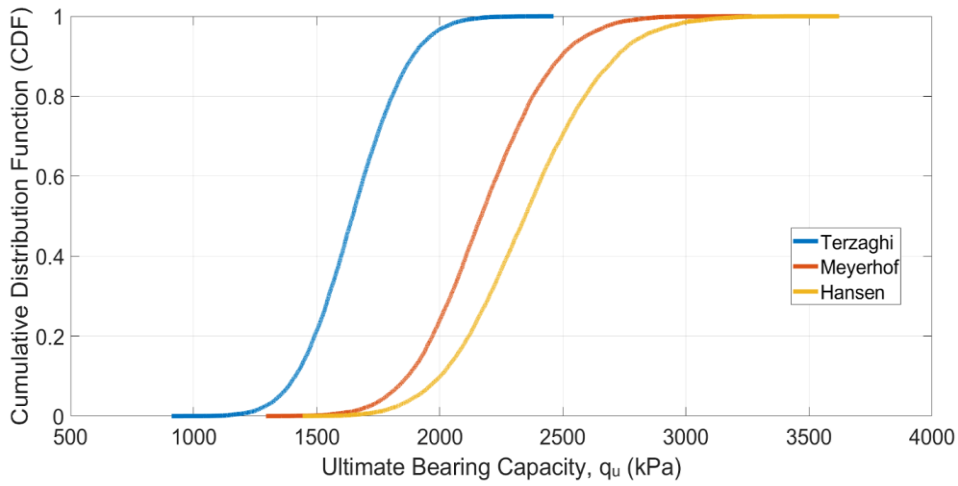

(a)

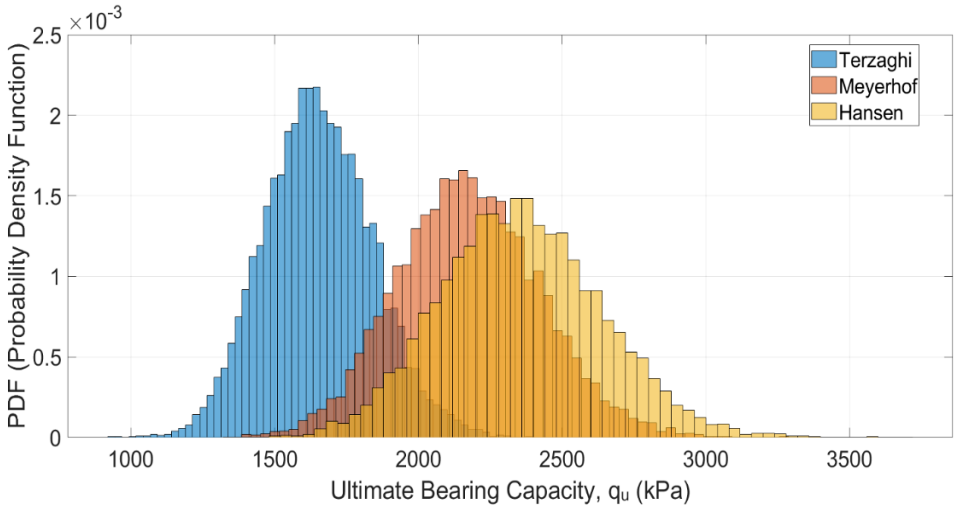

(b)

Figure 13. (a) Probability Density Function (PDF) of Uncorrected Lognormally Distributed Cohesion, (b) Cumulative Distribution Function (CDF) of Uncorrected Lognormal Cohesion

Equally critical is the probability distribution assumption for soil parameters. Normal distributions, though mathematically tractable, permit negative realizations of c and φ, which are physically implausible and potentially hazardous in reliability-sensitive design. By contrast, lognormal distributions enforce non-negativity and introduce right-skewness, thereby producing longer upper tails and more conservative estimates of extreme low-capacity scenarios. This distinction is visually evident in the divergence between normal and lognormal probability density and cumulative distribution functions prior to correction (Figures 12 and 13). The findings confirm that mischaracterization of parameter distributions can lead to systematic underestimation of failure probabilities, a risk particularly pronounced for critical foundations.

To address discrepancies between deterministic predictions and experimental data, regression-based calibration factors (λ) were applied, following the relation $qu_{corr} = \lambda \cdot qu$. As summarized in Table 1, calibration significantly improved alignment with empirical observations: bias was reduced, distribution peaks shifted toward experimental means (Figure 14), and probability spreads narrowed substantially (Figure 15). Among the models, Terzaghi demonstrated the strongest statistical consistency after correction (R^2=0.742), followed by Hansen and Meyerhof, as confirmed by regression plots (Figure 16). These results underscore the dual benefit of calibration both in mitigating systematic bias and in providing a more realistic representation of uncertainty. Overall, the evidence demonstrates that neither deterministic formulations nor probabilistic distributions alone are sufficient to ensure reliable geotechnical predictions. Instead, it is the integrated application of model choice, probabilistic characterization, and calibration that enables realistic and safety-oriented capacity estimates. For nanomaterial-stabilized soils, this combined approach is essential for mitigating the risk of underestimation and ensuring robust design in infrastructure projects with minimal tolerance for failure.

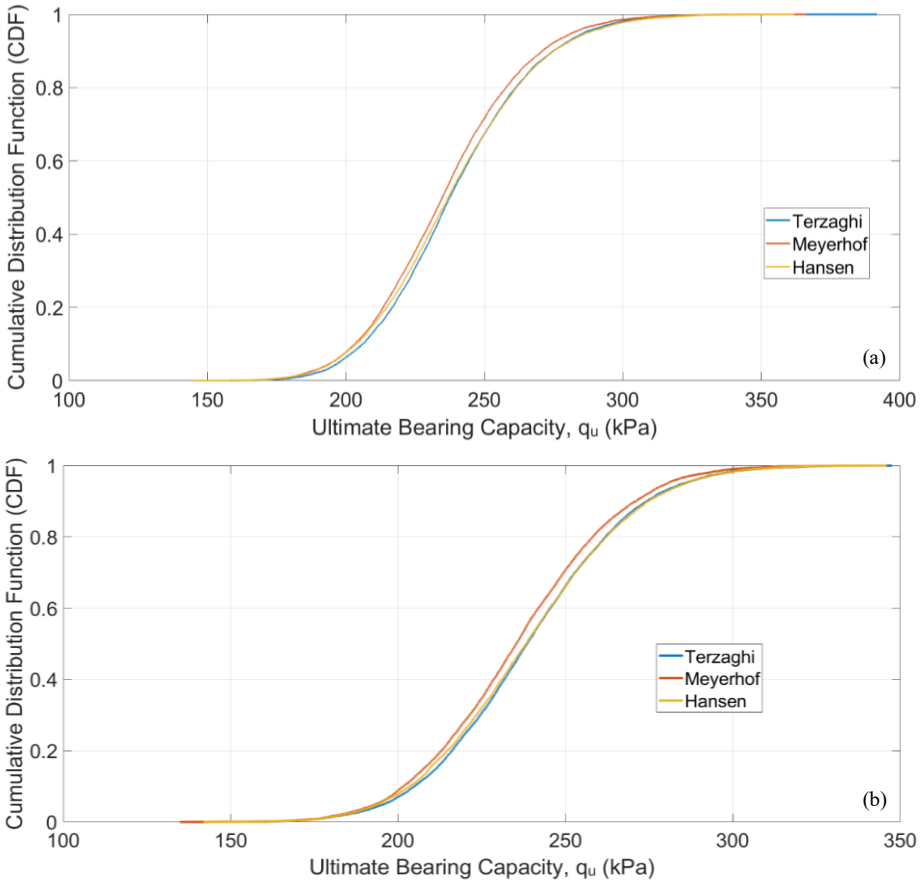

Figure 14. (a) Corrected Cumulative Distribution Function (CDF) of Cohesion Normal Distribution, (b) Corrected Cumulative Distribution Function (CDF) of Cohesion Lognormal Distribution

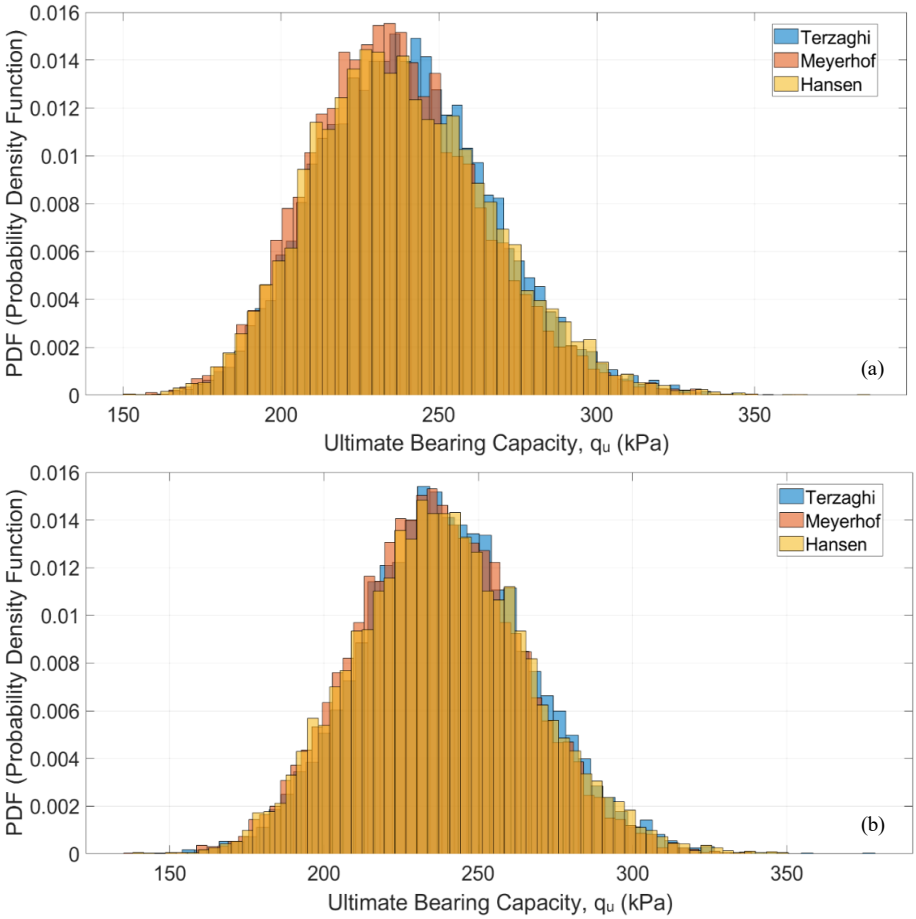

Figure 15. (A) PDF of Cohesion Normal (Corrected), (B) PDF of Cohesion Lognormal (Corrected)

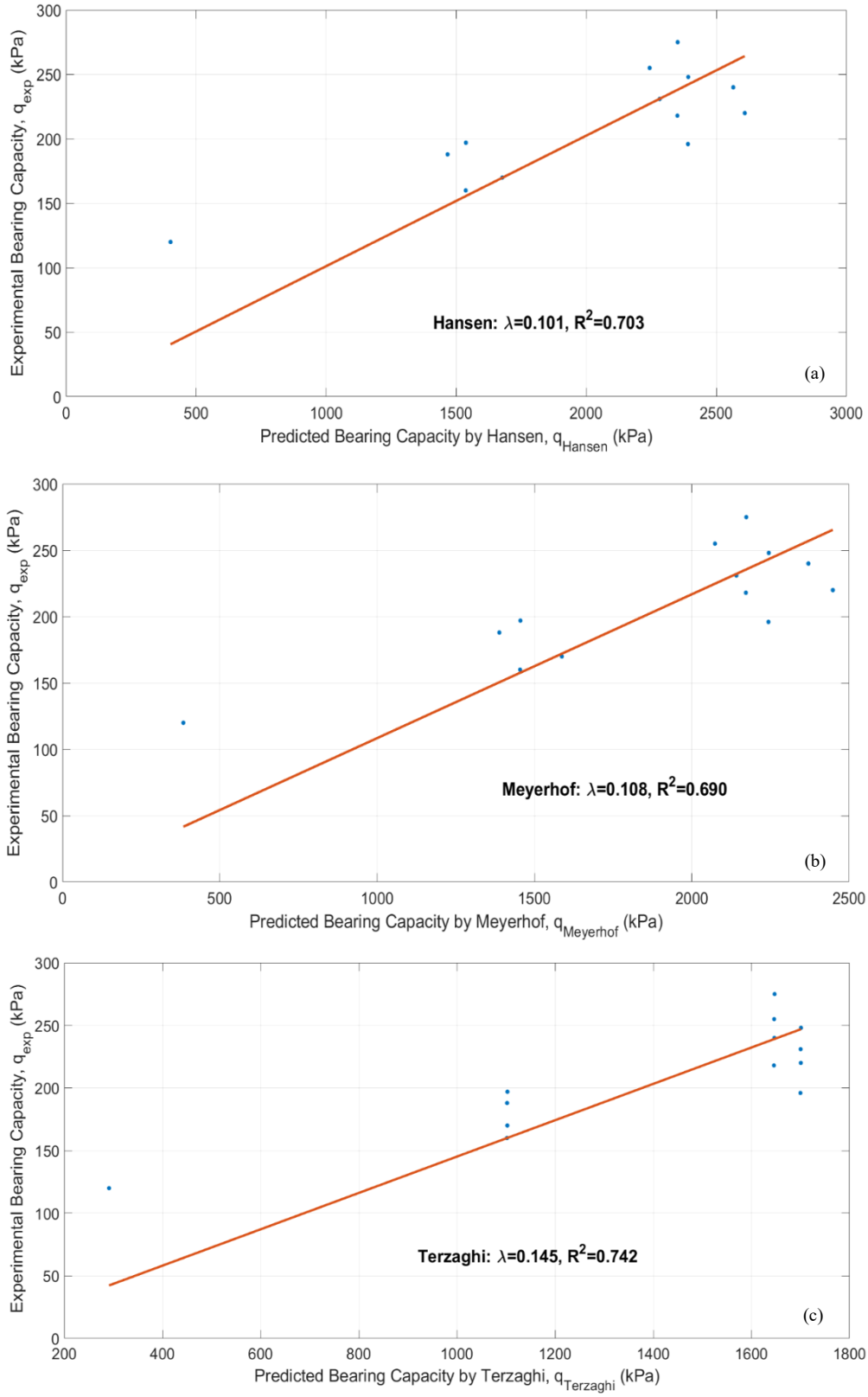

Figure 16. (a) Regression Analysis for Hansen Model, (b) Regression Analysis for Meyerhof Model, (c) Regression Analysis for Terzaghi Model

6.2. Reliability Assessment Across Nanomaterials and Geometries

The reliability analysis, expressed through the probability of failure (Pf) obtained via Monte Carlo simulations, reveals critical interactions between the type of nanomaterial used for soil stabilization, the geometry of the treated zone, and the adopted analytical model. As illustrated in Figures 17-A to 17-C, distinct patterns emerge across the three investigated nanomaterials—Nano Clay, Nano MgO, and Nano SiO_2 under four geometric configurations (Cases 1–4).

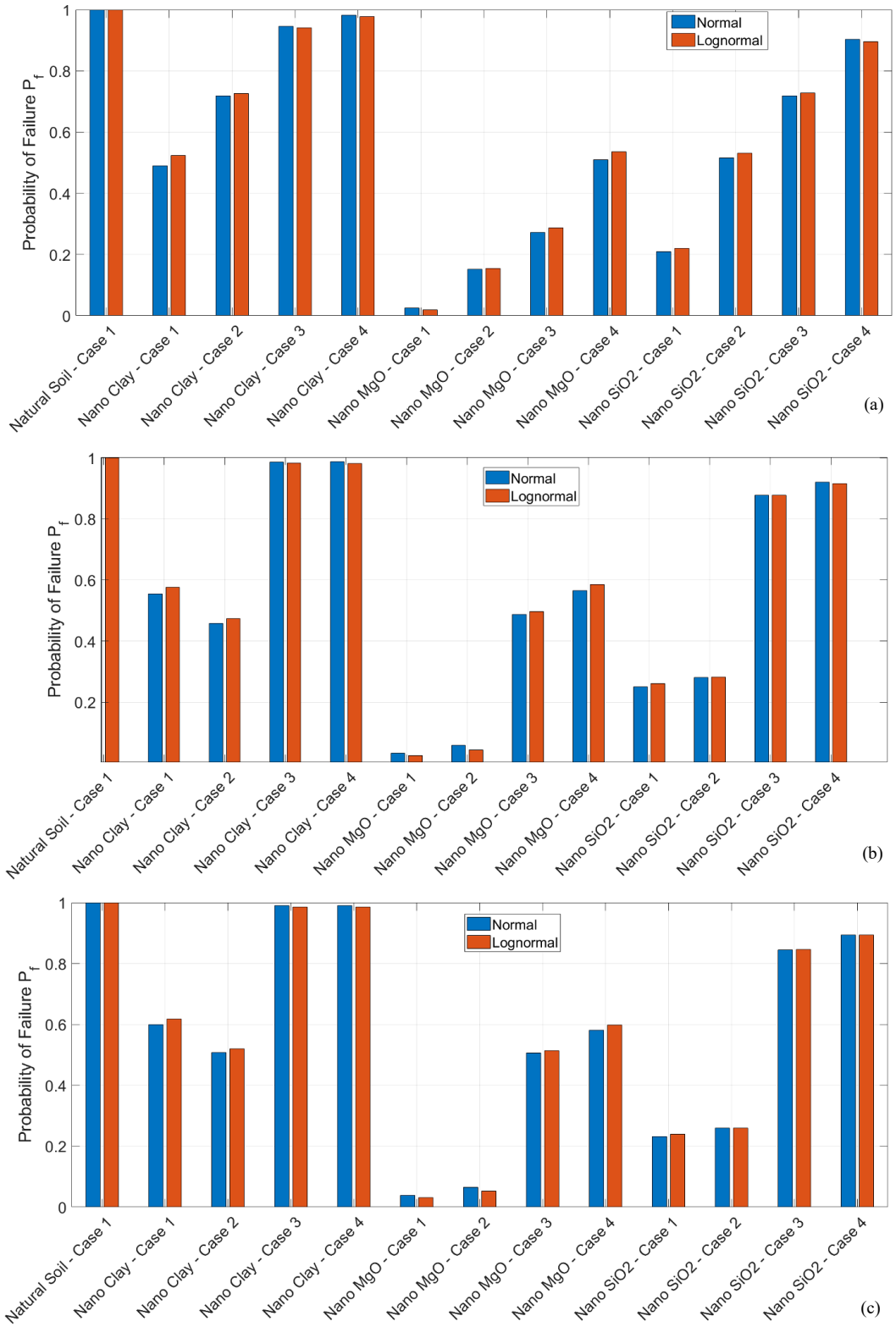

Figure 17. Probability of Failure (Pf) for different soil improvement cases using Normal and Lognormal distributions: (a) Based on Terzaghi Model, (b) Based on Meyerhof Model, (c) Based on Hansen Model

Material-specific performance was markedly differentiated. Nano-MgO consistently delivered the lowest failure probabilities across all models and geometries, with Case 1 (B×B/2 configuration) yielding ($Pf < 0.1\ Pf$) irrespective of the assumed probability distribution. This stability under uncertainty confirms Nano-MgO's superior strengthening capacity, reflecting both its physicochemical interaction with soil particles and its effectiveness in homogenizing stress transfer. Nano-SiO_2 demonstrated intermediate reliability, with Pf values ranging between ~ (0.2 and 0.8) depending on geometry and analytical formulation. Although laboratory tests confirm the promising mechanical enhancement achieved by Nano-SiO_2, the simulations highlight its greater sensitivity to geometry, indicating that design optimization

is essential for realizing its potential in field applications. By contrast, Nano Clay provided only limited improvements in reliability. In Cases 3 and 4, Pf values approached or even exceeded 0.9 across all models, suggesting that its effectiveness is highly contingent upon factors such as dispersion quality, mixing uniformity, and construction control, which are difficult to guarantee in practical field conditions.

Geometric effects were equally decisive in shaping reliability outcomes. Larger treated zones, particularly Case 4 (2B × 2B), consistently exhibited lower failure probabilities, reflecting improved stress redistribution and mitigation of localized overstressing. Conversely, configurations with smaller influence zones, such as Case 3, exhibited much higher Pf, underscoring the necessity of matching material type with an appropriate geometric treatment strategy. This interaction highlights the synergistic role of geometry and material in soil improvement design: even highly effective nanomaterials cannot offset the reliability losses associated with poorly optimized geometrical configurations.

Finally, distributional sensitivity analysis indicates that lognormal assumptions generally produce slightly more conservative estimates of Pf compared with normal distributions. The average deviation was typically within 5%, yet such differences become non-negligible in borderline safety scenarios, particularly where design safety factors are marginal. This result reaffirms the critical role of accurate probabilistic modeling in reliability-based design, ensuring that subtle statistical misrepresentations do not translate into substantial safety risks in practice.

In summary, the findings emphasize that Nano-MgO combined with appropriately enlarged treatment geometries (e.g., Case 4) provides the most robust improvement strategy under uncertainty. Conversely, reliance on Nano Clay, especially in smaller or less optimized geometries, is associated with unacceptably high failure probabilities, potentially compromising design safety. The results demonstrate that nanomaterial selection, geometric optimization, and distributional fidelity must be jointly considered to ensure reliable and resilient geotechnical performance.

7. Design Implications, Model Performance, and Research Recommendations

The integration of probabilistic modeling, statistical calibration, and material-specific performance assessment provides a robust foundation for reliability-based geotechnical design in nanomaterial-stabilized soils. The findings clearly demonstrate that reliance on deterministic values of ultimate bearing capacity (qu) may lead to significant misrepresentation of risk either by underestimating the likelihood of failure or by producing overly conservative designs that compromise economic feasibility. Incorporating empirically derived correction factors (λ) shifts the design process from idealized predictions toward more realistic and field-representative estimates, thereby enhancing both accuracy and safety.

Regression analyses (Figure 15) confirm the comparative performance of the classical models. The calibrated Terzaghi formulation exhibits the strongest agreement with experimental data (R^2=0.742), balancing simplicity with statistical reliability. Hansen's model shows a reasonable fit (R^2=0.703) but introduces greater variability due to its sensitivity to additional geometric and loading parameters. Meyerhof's model, while moderately predictive (R^2=0.69), tends to overestimate capacities in certain configurations. Taken together, these results support the use of the calibrated Terzaghi model as a practical and dependable baseline for design under uncertainty, particularly in reliability-sensitive applications.

From a material perspective, Nano-MgO consistently emerges as the most effective stabilizer, delivering robust improvements in reliability across variable geometries and probabilistic conditions. Its performance underscores the importance of selecting nanomaterials not only based on laboratory strength gains but also on their reliability profiles under stochastic loading and soil variability. Nano-SiO_2 offers promising but geometry-sensitive outcomes, while Nano Clay demonstrates limited effectiveness, highlighting the critical role of microstructural interactions, dispersion quality, and field mixing conditions.

These insights motivate several key recommendations for advancing geotechnical practice and research:

- Adoption of Probabilistic Limit State Design (PLSD): Updating geotechnical design codes to incorporate probabilistic methods will better capture inherent uncertainties and reduce the risks associated with purely deterministic approaches.
- Bayesian Updating for Parameter Refinement: Future studies should integrate Bayesian frameworks to progressively refine input parameter distributions as additional experimental and field data become available.
- Microstructural Investigations: Detailed studies of the physicochemical interactions between nanomaterials and clay matrices are needed to reduce epistemic uncertainty and to identify mechanisms that drive performance variability.
- Optimization of Treatment Geometry: The geometry of the improved zone must be tailored to each nanomaterial to maximize stress redistribution and reliability, recognizing that material effectiveness is strongly geometry-dependent.

- Long-Term Durability: The long-term performance of nano-stabilized soils remains an open question. Future research should evaluate durability under cyclic environmental loading such as wetting–drying and freeze–thaw cycles, to ensure that short-term gains in strength and stiffness translate into sustainable improvements in service life.
- Blending Strategies: The potential for hybrid nanomaterial systems, particularly combinations such as Nano-SiO_2 and Nano-MgO, warrants investigation. Such blends may offer synergistic benefits by combining the high strength gains of silica with the reliability and stability of MgO, thereby broadening the design envelope for challenging soil conditions.
- Scalability and Field Application: While laboratory-scale and model footing experiments demonstrate promising outcomes, the scalability of these treatments to large infrastructure projects (e.g., ports, highways, and embankments) requires careful consideration. Issues of cost, mixing uniformity, and quality control must be addressed to ensure consistent performance in real-world conditions.

8. Conclusion

This study demonstrates that the integration of experimental evidence with probabilistic modeling provides a robust framework for designing shallow foundations on nano-stabilized clays. The combination of triaxial and model footing tests with calibrated bearing capacity models and Monte Carlo simulations enabled a more realistic assessment of reliability compared to deterministic approaches. The results highlight that Nano-MgO is the most effective stabilizer, consistently achieving the lowest probability of failure across varying geometries, while Nano-SiO_2 offers substantial improvements that remain sensitive to treatment configuration. Nano-Clay showed only modest enhancements, indicating limited applicability where reliability margins are critical. Enlarged treatment zones were found to significantly improve stress redistribution and reduce failure risk, underscoring the importance of geometric optimization in soil improvement design. Among the classical formulations, the calibrated Terzaghi model ($R^2 = 0.742$) exhibited the strongest agreement with experimental data, providing a practical and statistically consistent baseline for reliability-centered design. These findings confirm that reliance on deterministic models alone may misrepresent geotechnical risk, whereas calibrated probabilistic methods ensure safer and more economical foundation solutions in soft clays stabilized with nanomaterials.

9. Declarations

9.1. Author Contributions

Conceptualization, M.Y.F. and N.I.M.P.; methodology, F.K.K.; software, F.K.K.; validation, F.K.K., M.Y.F., and N.I.M.P.; formal analysis, F.K.K.; investigation, F.K.K.; resources, K.S.M.; data curation, M.H.H.; writing—original draft preparation, F.K.K.; writing—review and editing, M.Y.F.; visualization, N.S.; supervision, N.I.M.P.; project administration, M.Y.F.; funding acquisition, K.S.M. All authors have read and agreed to the published version of the manuscript.

9.2. Data Availability Statement

The data presented in this study are available in the article.

9.3. Funding

The authors received no financial support for the research, authorship, and/or publication of this article.

9.4. Conflicts of Interest

The authors declare no conflict of interest.

10. References

[1] Gu, J., Cai, X., Wang, Y., Guo, D., & Zeng, W. (2022). Evaluating the Effect of Nano-SiO2 on Different Types of Soils: A Multi-Scale Study. International Journal of Environmental Research and Public Health, 19(24), 16805. doi:10.3390/ijerph192416805.

[2] Hu, P., Chen, S., Duan, Z., Wang, N., Hao, Y., & Wang, X. (2025). Effect of freeze-thaw cycles on mechanical performance of loess soil stabilized with nano magnesium oxide. PLOS One, 20(4), e0319909. doi:10.1371/journal.pone.0319909.

[3] Arabani, M., Shalchian, M. M., & Majd Rahimabadi, M. (2023). The influence of rice fiber and nanoclay on mechanical properties and mechanisms of clayey soil stabilization. Construction and Building Materials, 407, 133542. doi:10.1016/j.conbuildmat.2023.133542.

[4] Cheraghalikhani, M., Niroumand, H., & Balachowski, L. (2023). Micro- and nano- bentonite to improve the strength of clayey sand as a nano soil-improvement technique. Scientific Reports, 13(1), 10913. doi:10.1038/s41598-023-37936-x.

[5] P. Dukuly, L., Ghani, S., & Kushwaha, S. (2025). Experimental and Numerical Study on Nano-Silica-Stabilized Clayey Subgrades with Geogrid Support. Transportation Infrastructure Geotechnology, 12(5), 156. doi:10.1007/s40515-025-00612-w.

[6] Hassan Al-Riahi, S. M., Irfah Mohd Pauzi, N., Fattah, M. Y., & Ali Abbas, H. (2024). Leaching-induced alterations in the geotechnical and microstructural attributes of clayey gypseous soils. Ain Shams Engineering Journal, 15(7), 102865. doi:10.1016/j.asej.2024.102865.

[7] Pauzi, N.I.M., Aimran, M.A., Ismail, M.S., Radhi, M.S.M. (2020). Optimization of Egg Shell Powder and Lime for Waste Soil Improvement at Open Dumping Area Using Monte Carlo Simulations. Lecture Notes in Civil Engineering, Springer, Cham, Switzerland. doi:10.1007/978-3-030-32816-0_3.

[8] Sharmile, N., Chowdhury, R. R., & Desai, S. (2025). A Comprehensive Review of Quality Control and Reliability Research in Micro–Nano Technology. Technologies, 13(3), 94. doi:10.3390/technologies13030094.

[9] Zhou, Z., Ma, W., Zhang, S., Mu, Y., & Li, G. (2020). Experimental investigation of the path-dependent strength and deformation behaviours of frozen loess. Engineering Geology, 265, 105449. doi:10.1016/j.enggeo.2019.105449.

[10] Lei, B., Zhang, X., Fan, H., Gao, J., Du, Y., Ji, Y., & Gao, Z. (2025). Effects of Nano-SiO2 and Nano-CaCO3 on Mechanical Properties and Microstructure of Cement-Based Soil Stabilizer. Nanomaterials, 15(11), 785. doi:10.3390/nano15110785.

[11] Alshami, A. W., Ismael, B. H., Aswad, M. F., Majdi, A., Alshijlawi, M., Aljumaily, M. M., AlOmar, M. K., Aidan, I. A., & Hameed, M. M. (2022). Compaction Curves and Strength of Clayey Soil Modified with Micro and Nano Silica. Materials, 15(20), 7148. doi:10.3390/ma15207148.

[12] Phoon, K.-K., & Tang, C. (2019). Characterisation of geotechnical model uncertainty. Georisk: Assessment and Management of Risk for Engineered Systems and Geohazards, 13(2), 101–130. doi:10.1080/17499518.2019.1585545.

[13] Baecher, G. B. (2023). 2021 Terzaghi Lecture: Geotechnical Systems, Uncertainty, and Risk. Journal of Geotechnical and Geoenvironmental Engineering, 149(3). doi:10.1061/jggefk.gteng-10201.

[14] ASTM D854-14. (2023). Standard Test Methods for Specific Gravity of Soil Solids by Water Pycnometer. ASTM International, Pennsylvania, United States. doi:10.1520/D0854-14.

[15] ASTM D422-63(2007). (2014). Standard Test Method for Particle-Size Analysis of Soils. ASTM International, Pennsylvania, United States. doi:10.1520/D0422-63R07.

[16] ASTM D4943-08. (2018). Standard Test Method for Shrinkage Factors of Soils by the Wax Method. ASTM International, Pennsylvania, United States. doi:10.1520/D4943-08.

[17] ASTM D4318-00. (2017). Standard Test Methods for Liquid Limit, Plastic Limit, and Plasticity Index of Soils. ASTM International, Pennsylvania, United States. doi:10.1520/D4318-00.

[18] ASTM D698-12(2021). (2021). Standard Test Methods for Laboratory Compaction Characteristics of Soil Using Standard Effort (12,400 ft-lbf/ft^3 (600 kN-m/m^3)). ASTM International, Pennsylvania, United States. doi:10.1520/D0698-12R21.

[19] ASTM D2487-17e1. (2025). Standard Practice for Classification of Soils for Engineering Purposes (Unified Soil Classification System). ASTM International, Pennsylvania, United States. doi:10.1520/D2487-17E01.

[20] BS 1377: 1990. (1990). Methods of test for soils for civil engineering purposes. British Standards Institution (BSI), London, United Kingdom.

[21] Head, K. H., & Epps, R. J. (1998). Manual of soil laboratory testing. Volume 3: effective stress tests. John Wiley, Hoboken, United States.

[22] ASTM D5907-18. (2025). Standard Test Methods for Filterable Matter (Total Dissolved Solids) and Nonfilterable Matter (Total Suspended Solids) in Water. ASTM International, Pennsylvania, United States. doi:10.1520/D5907-18.

[23] ASTM D512-23. (2023). Standard Test Methods for Chloride Ion In Water. ASTM International, Pennsylvania, United States. doi:10.1520/D0512-23.

[24] ASTM D2974-14. (2020). Standard Test Methods for Moisture, Ash, and Organic Matter of Peat and Other Organic Soils. ASTM International, Pennsylvania, United States. doi:10.1520/D2974-14.

[25] Kalhor, A., Ghazavi, M., & Roustaei, M. (2022). Impacts of Nano-silica on Physical Properties and Shear Strength of Clayey Soil. Arabian Journal for Science and Engineering, 47(4), 5271–5279. doi:10.1007/s13369-021-06453-2.

[26] Ibrahim, M., Johari, M. A. M., Maslehuddin, M., & Rahman, M. K. (2018). Influence of nano-SiO2 on the strength and microstructure of natural pozzolan based alkali activated concrete. Construction and Building Materials, 173, 573–585. doi:10.1016/j.conbuildmat.2018.04.051.

[27] Abdulamer, H. N., & Daham, H. A. (2025). Geotechnical Study of Expansive Soil Treated with Nano-Calcium Carbonate Materials in Al-Faw City, Southern Iraq. Tikrit Journal of Engineering Sciences, 32(1), 1–8. doi:10.25130/tjes.32.1.14.

[28] Regalla, S. S. (2024). Effect of nano SiO2 on rheology, nucleation seeding, hydration mechanism, mechanical properties and microstructure amelioration of ultra-high-performance concrete. Case Studies in Construction Materials, 20, e03147. doi:10.1016/j.cscm.2024.e03147.

[29] Yao, K., An, D., Wang, W., Li, N., Zhang, C., & Zhou, A. (2020). Effect of nano-MgO on mechanical performance of cement stabilized silty clay. Marine Georesources & Geotechnology, 38(2), 250–255. doi:10.1080/1064119X.2018.1564406.

[30] Khayat, N., Ohadian, A., & Mokhberi, M. (2023). Long-term and microstructural studies of soft clay stabilization using municipal solid waste and Nano-MgO as an Eco-Friendly Method. Anthropogenic Pollution, 7(1), 35-54.